Available online at www.sciencedirect.com

ScienceDirect

Geochimica et Cosmochimica Acta 121 (2013) 637–651

Geochimica et Cosmochimica Acta

www.elsevier.com/locate/gca

The riverine silicon isotope composition of the Amazon Basin

H.J. Hughes [a,*], F. Sondag [b], R.V. Santos [c], L. André [a], D. Cardinal [a,d]

[a] Dept. of Geology and Mineralogy, Royal Museum for Central Africa, Tervuren, Belgium
[b] GET (Université de Toulouse III, CNRS, IRD), Brasilia, Brazil
[c] Laboratory of Geochronology, University of Brasilia, Brasilia, Brazil
[d] Laboratoire d'Océanographie et du Climat: Expérimentations et Approches Numériques, IRD/UPMC/MNHN/CNRS, IPSL, Université Pierre et Marie Curie, Paris, France

Received 17 August 2012; accepted in revised form 31 July 2013; available online 9 August 2013

Abstract

We present here the first large-scale study of riverine silicon isotope signatures in the Amazon Basin. The Amazon and five of its main tributaries were studied at different seasons of the annual hydrological cycle. The $\delta^{30}Si$ signature of the dissolved silicon (DSi) exported to the estuary (weighted for DSi flux) for the period considered is estimated at +0.92‰. A river cross-section shows the homogeneity of the Amazon River regarding DSi concentration and isotope ratio. The biogenic silica (BSi) concentration measured in surface water from all rivers is generally small compared to the DSi reservoir but large variations exist between rivers. Very low isotope signatures were measured in the upper Rio Negro ($\delta^{30}Si = +0.05 \pm 0.06$‰), which we explain both by an equilibrium between clay formation and dissolution and by gibbsite formation. The Si isotope fractionation in the Andean tributaries and the Amazon main stem can be explained by clay formation and follow either a Rayleigh or a batch equilibrium fractionation model. Our results also suggest that the formation of 2:1 clays induces a fractionation factor similar to that of kaolinite formation.

1. INTRODUCTION

Silicon is a ubiquitous element and has complex interactions with the biogeochemical cycles of other elements. The Si cycle exerts an influence on the carbon cycle through the weathering of primary silicate, which consumes CO_2 and converts it to dissolved HCO_3^-. This mechanism is thought to be one of the main factors driving the long-term variations of the concentration of atmospheric CO_2 (e.g., Berner et al., 1983; Bluth and Kump, 1994). Dissolved silicon (in the form of orthosilicic acid H_4SiO_4, thereinafter referred to as DSi) is also an important nutrient in aquatic systems. Changes in the DSi flux of rivers have a significant impact on the coastal primary productivity and ecosystems (Garnier et al., 2010), where diatoms consume Si to build their frustules. These algae account for 75% of the primary production in coastal areas (Nelson et al., 1995) and therefore have an important role in the export of C to sediment (Tréguer and Pondaven, 2000).

Si isotope signatures in rivers have recently been proved to be useful for tracing the different processes affecting the continental biogeochemical cycle of Si, such as clay formation (Georg et al., 2007), mixing of DSi from different sources (Georg et al., 2006a), biological uptake (Ding et al., 2004; Engström et al., 2010), and is sensitive to anthropogenic impact (Hughes et al., 2012) and land-use (Delvaux et al., in press). In tropical rivers, Si isotopes have recently been used to quantify Si inputs from rivers that are rich in dissolved organic matter into the Congo River ("black rivers"; Cardinal et al., 2010) and to estimate the

* Corresponding author. Address: Royal Museum for Central Africa, Leuvensesteenweg, 13, B-3080 Tervuren, Belgium. Tel.: +32 2 769 54 01; fax: +32 2 769 54 32.
E-mail address: harold.hughes@africamuseum.be (H.J. Hughes).

0016-7037/$ - see front matter © 2013 Elsevier Ltd. All rights reserved.
http://dx.doi.org/10.1016/j.gca.2013.07.040

production of diatoms (Hughes et al., 2011a). Tropical rivers generally have high DSi concentrations as a result of their geological and climatic settings (Jennerjahn et al., 2006; Beusen et al., 2009) and are the main suppliers of DSi to the ocean (Tréguer and De La Rocha, 2013). With a mean annual discharge of about 200,000 m^3/s, the Amazon River is estimated to represent up to 20% of the worldwide riverine water flux to the oceans (Richey et al., 1989; Milliman, 2001; Callède et al., 2010) and 11% of the global riverine DSi export to the oceans (Beusen et al., 2009). The Si cycle in its watershed is therefore of importance at global scale. Given the importance of these exports, the determination of the isotope signature of the Amazon would also be of interest for the use of Si isotopes in marine sciences. Our aim is to better understand the factors that drive the DSi isotope compositions in the Amazon Basin.

2. DESCRIPTION OF THE STUDY AREA

2.1. Geology and geomorphology

The Amazon Basin is the world's largest watershed and covers an area of 6.1 million km^2 occupied for more than 96% of its surface by silicate rocks (Amiotte-Suchet et al., 2003). Stallard and Edmond (1983) divided the basin into four contrasted morphostructural units (Fig. 1): the Andean Cordillera (west and southwest), the Sub-Andean area, the Guiana and Brazilian cratonic shields and the Amazon Trough. (a) The Andean Cordillera has a complex and heterogeneous lithology. This region consists primarily of zones of high relief constituted of sedimentary and igneous rocks metamorphosed to varying degrees. A distinction can be made between the Peruvian part (North), drained by the Andean Solimões Basin and the Bolivian part (South) drained by the Andean Madeira Basin. The Andean Solimões Basin drains a large variety of rocks, including evaporites, carbonates, and volcanic rocks (in the northernmost part). These evaporite and carbonates control the chemistry (cations and anions) of the Amazon downstream (Moquet et al., 2011). The Andean Madeira Basin on the contrary mainly drains sedimentary rocks and few evaporites. (b) The Sub-Andean area constitutes the transition zone between the Andean Cordillera and the Amazon Trough. Due to the high precipitation and to the steep topographic gradient, the Andean chain is subject to intensive erosion and brings an enormous quantity of sediments to the Andean tributaries of the Amazon River (2.3–3.1 Gt/yr; Aalto et al., 2006); the rapid decrease of the slope in the Sub-Andean area favors a high rate of sedimentation and about half the sediments originating from the Andes accumulate in this zone. (c) The Brazil and Guiana Shields are developed on Precambrian Crystalline rocks. Their lithology mainly includes granite, granodiorite and microgranite and the soils tend to be several tens of meters thick (Lucas, 2001). (d) The Amazon Trough corresponds to the lowland area. It has a very weak slope and is covered by Tertiary and Quaternary lacustrine and alluvial deposits often weathered to clays. The Tertiary fluvio-lacustrine sediments of the Amazon Trough and the soils of the shields are products of intense weathering and are extremely depleted in cations (Stallard and Edmond, 1983). In this lowland area, floodwater and direct precipitation annually inundate about 40,000 km^2 of floodplain. Regarding the forested area, even though large zones have been cut in the southern and eastern margin of the basin in the course of the last decades, the Amazon Basin remains mainly covered by a rather uniform tropical rainforest cover with some small areas dominated by savannahs (Mertes and Dunne, 2007).

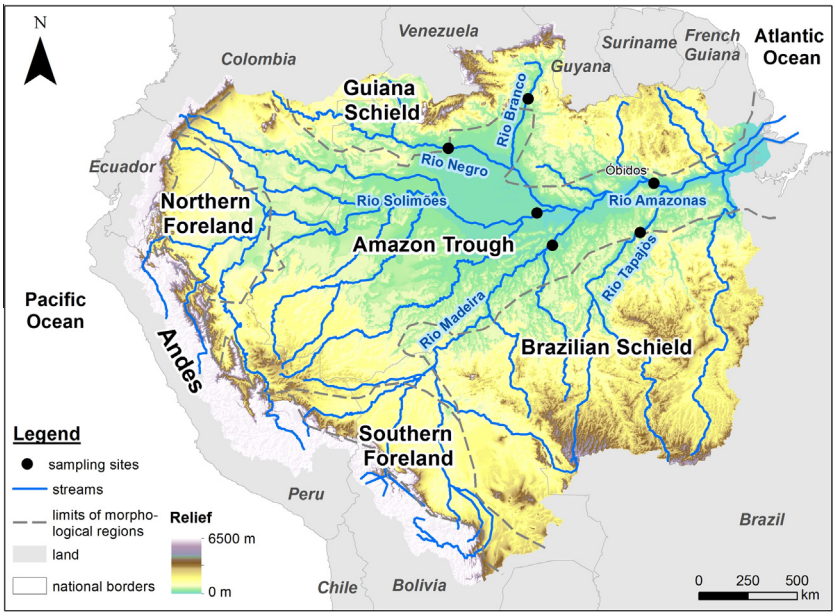

Fig. 1. Map of the Amazon Basin showing the sampling locations and the main geomorphological units. Watershed limit (Callède et al., 2010) and hydrographic network (Muller et al., 1999) taken from www.ore-hybam.org. Limits of geomorphological units provided courtesy of J.-S. Moquet.

2.2. River types and hydrology

In this study, as the physico-chemical characteristics of the main tributaries of the Amazon tally with the morpho-structural units, a geographical terminology will be used. Andean rivers are rich in dissolved and suspended material and their pH is close to neutrality. They are mainly represented by rivers draining the Andes and the Sub-Andean area, but also include the larger rivers downstream (e.g., Madeira and Solimões) and strongly impact the chemistry of the Amazon main stem. In their mountainous part, these rivers correspond to a highly weathering-limited regime (Stallard and Edmond, 1987). Clay minerals with a 2:1 structure are abundant in sediments in these rivers, but kaolinite is also found in the suspended load (Stallard and Edmond, 1987; Guyot et al., 2007). Shield rivers originate on the plateaus from the Guiana and Brazilian Shields (e.g., Tapajós, Xingú, Branco). They are colorless, highly transparent and depleted in dissolved material. Their pH vary from neutral to acid (<5.5). Their slope is moderate, except when crossing the edge of the plateau. This gentle slope and the hardness of the rocks from the shields explain the small amount of suspended matter and the very low erosion rate. A study from rivers draining the Guiana Shield showed that in these basins the intense weathering produces mostly kaolinite and gibbsite (Edmond et al., 1995), which is consistent with the minerals observed in these rivers (Guyot et al., 2007). Finally, black rivers are common in the flat and forested area from lowland parts of the Amazon Basin, where the soils are always wet or seasonally inundated. They are intensely colored by humic substances from the forest soils they drain. This high humic acid content is responsible for the low pH, comprised between 3.8 and 4.9. They drain extremely weathered and thick soils, mainly podzols, which contain an important quartz fraction (Dubroeucq and Volkoff, 1998). They are more diluted than shield rivers and the leaching of soluble cations from soil is complete (Edmond et al., 1995). Like shield rivers they represent an extreme example of transport-limited weathering and therefore have low suspended matter contents (Stallard and Edmond, 1983).

North from the equator (mainly the Rio Negro Basin), the maximum rainfall is observed from May to July, while in the southern part of the basin the maximum rainfalls are mainly from December to March. The combination of the multiple floods associated to the large drainage area and the buffering effect of the floodplain lead together to one great annual flood wave with a maximum flow spread from April to July inducing a 7 to 10 m rise and fall in the main stem (Pardé, 1947; Richey et al., 1989). Although the total volume of water annually drained from the floodplain is small compared to the annual discharge of the Amazon (ca. 5%; Alsdorf et al., 2010) it was estimated to represent up to 25% of the water discharge at Óbidos during the low flow period (Richey et al., 1989). The mean river discharge at Óbidos remains almost constant at 175,000 m^3/s for the period 1995–2007 (Martinez et al., 2009). Before 2001, the annual mean sediment discharge at this station was approximately 688×10^6 t/yr, while for the 2001–2007 period, it increased to 801×10^6 t/yr (Martinez et al., 2009). This increase was attributed to more intense erosion processes caused by changes either at the global scale (like rainfall), or at the regional scale (deforestation and land cover change). Note that no major river from the basin is currently dammed (Tollefson, 2011).

3. SAMPLING AND ANALYTICAL METHODS

3.1. Sampling and hydro-chemical parameters

In order to study temporal and spatial variations of the $\delta^{30}Si$ ratio in DSi, different batches of samples were considered. Six samples from the Amazon main stem (station Óbidos), collected from May 2010 to November 2010, were analyzed. Samples from 5 tributaries (see Fig. 1), representative of different types of rivers of the Amazon Basin and corresponding to different phases of the hydrological cycle – depending on the aliquots available – were also analyzed (Table 1). The samples were collected within the framework of the ORE-HYBAM program (Observatoire de Recherche sur l'Environnement – Hydrologie du Bassin Amazonien). Areas and discharges of the rivers are provided in Table 1. The samples were collected at the water subsurface in the middle of the stream, filtered onto 0.22 μm cellulose nitrate filters and stored unacidified in HDPE bottles. The filters themselves were kept for biogenic silica (BSi) contents analyses. A database for hydrological and geochemical data is provided by the ORE-HYBAM program (http://www.ore-hybam.org). As large rivers of the Amazon Basin have been shown to be sometimes poorly mixed and influenced by lateral inflow (Bouchez et al., 2010), a group of samples collected at Óbidos along the river width and a depth profile are also studied in order to check the homogeneity of the section. These samples were collected on 2nd July 2010 following the same protocol as detailed above. The concentrations of major cations and DSi were measured by inductively coupled plasma optical emission spectrometry (ICP-OES) except for the cross-section samples for which DSi was measured colorimetrically by the molybdenum-blue method; major anions (F^-, Cl^-, NO_3^-, PO_4^{3-}, SO_4^{2-}) were determined using ion chromatography. Samples of siliceous sponges were collected in August 2010 on a tree trunk just below the water surface in the Rio Negro near Manaus.

3.2. Biogenic silica

The concentration of BSi in suspended matter was estimated using a wet alkaline digestion on the particles collected on the filters following the method of Ragueneau et al. (2005). A first leaching in 0.2 mol/L NaOH at 100 °C for 40 min is applied to a fraction of the filter. After this first step, all the BSi and an unknown amount of lithogenic silica (LSi) were dissolved. The filter was rinsed and dried and then submitted to a second digestion step. Si and Al concentrations were then measured in the resulting leaching solution using an inductively coupled plasma mass spectrometer (XSERIES-2, Thermo Scientific). The Al:Si ratio measured in the second leaching solution is then used to correct for the LSi contamination during the first

Table 1
Samples characteristics and geochemical data. The water flow rate is the value observed for the day of sampling. BSi is the amount of biogenic silica measured on the filters and % BSi indicate the % of BSi in the total Si (sum of DSi and BSi). σ_{SD} on isotopic ratio is given as the standard deviation on the replicates; where only one analysis could be done (italic values) the average analytical standard error is given. AR, SR, and BW indicate Andean river, Shield river and black water, respectively. <D.L. denotes a value below detection limit. *Indicate data corrected for atmospheric inputs and evaporite dissolution. The + on Cl data indicate that the Cl concentration of the following month was used (cf. Section 4.1). f_{Si} is the Si mobility (see text for details).

Samples	Basin area	DSi	BSi	% BSi	Ca	Mg	Na	K	Cl	Ca*	Mg*	Na*	K*	f_{Si}	Discharge	Specific discharge	Specific DSi flux	$\delta^{30}Si$	$2\sigma_{SD}$	$\delta^{29}Si$	$2\sigma_{SD}$	n
	km^2	µmol/L		%	µmol/L					µmol/L					m^3/s	$m^3\ s^{-1}\ km^{-2}$	$mol\ yr^{-1}\ km^{-2}$	‰		‰		
Rivers																						
Amazon (AR)																						
May 2010	4,618,750	124	6.8	5.2	157	41	74	23	33	152	38	44	23	0.53	240,200	0.052	203,231	0.75	0.09	0.36	0.12	2
Jun 2010		120			144	37	74	21	35	139	34	42	21	0.54	239,700	0.052	196,588	0.71	0.17	0.36	0.06	4
Jul 2010		121	7.5	5.8	85	39	69	22	31	81	36	40	21	0.56	213,800	0.046	177,350	0.87	0.13	0.44	0.19	2
Sep 2010		130	9.9	7.1	65	39	74	21	35	60	35	42	21	0.59	120,300	0.026	106,403	0.90	0.15	0.42	0.21	2
Oct 2010		134			105	55	124	24	67	90	48	60	23	0.46	79,190	0.017	72,668	1.28	0.04	0.65	0.07	3
Nov 2010		145	12.4	7.9	165	78	179	30	94	141	70	88	28	0.35	75,840	0.016	74,993	1.76	0.25	0.89	0.17	5
Madeira (AR)																						
Jan 2010	1,324,700	155			126	71	79	39	19	126	69	63	38	0.43	31,750	0.024	117,329	0.83	0.06	0.43	0.04	2
Apr 2010		149	7.3	4.7	97	59	65	37	14	97	57	52	36	0.48	50,150	0.038	178,057	0.83	0.04	0.46	0.13	2
Jul 2010		161	1.6	1.0	140	80	102	31	26	137	77	74	30	0.44	13,810	0.010	53,070	1.17	0.17	0.57	0.20	2
Oct 2010		114	4.9	4.2	235	126	157	33	34	229	121	113	32	0.22	5,862	0.004	15,865	1.66	0.15	0.82	0.04	3
Solimões (AR)																						
Jan 2010	2,147,740	93			316	64	127	21	70	300	58	59	20	0.33	89,230	0.042	122,222	2.09	0.05	1.08	0.05	2
Apr 2010		82	11.6	12.3	300	54	119	21	63	286	48	58	20	0.30	118,100	0.055	142,567	2.28	0.16	1.13	0.07	3
Aug 2010		167	7.6	4.4	200	44	137	20	73	183	37	67	19	0.55	108,400	0.050	265,603	0.96	0.18	0.51	0.03	3
Oct 2010		191	13.4	6.5	308	70	272	25	168	261	54	106	22	0.42	27,050	0.013	75,921	1.41	0.11	0.73	0.10	3
Tapajós (SR)																						
Apr 2010	452,000	170	1.1	0.6	24	19	36	22	12	24	18	26	22	1.01	16,770	0.037	198,619	1.02	0.20	0.52	0.12	5
Jul 2010		146	<D.L.	<D.L.	39	18	40	26	6	38	17	35	26	0.69	2,400	0.005	24,496	0.71	0.29	0.32	0.02	4
Oct 2010		140	<D.L.	<D.L.	33	19	40	25	19	33	18	24	25	0.82	736	0.002	7,165	0.72	0.23	0.37	0.08	5
Branco (SR)																						
Jan 2010	124,980	245	2.2	0.9	55	47	114	35	27	54	45	101	35	0.55	559	0.004	34,544	1.37	0.16	0.68	0.06	4
Apr 2010		238	3.4	1.4	35	43	102	44	29	34	41	88	44	0.56	616	0.005	37,041	1.31	0.20	0.70	0.11	4
Jul 2010		192	0.4	0.2	41	30	63	27	16+	41	28	49	27	0.72	9,932	0.079	482,077	1.07	0.03	0.52	0.21	2
Oct 2010		231	1.5	0.6	41	33	84	31	14+	40	31	70	31	0.64	2,399	0.019	140,018	1.17	0.24	0.57	0.14	3
Negro (BW)																						
Jan 2010	279,950	65	0.3	0.5	4	2	20	10	12	4	1	10	10	0.93	15,000	0.054	109,022	−0.01	*0.14*	−0.02	*0.07*	1
Apr 2010		59	<D.L.	<D.L.	5	2	17	13	10	5	1	9	13	0.78	11,040	0.039	73,245	0.11	0.14	0.11	0.01	2
Jun 2010		52	<D.L.	<D.L.	8	3	14	10	5	8	2	9	10	0.78	25,150	0.090	148,401	0.06	*0.14*	0.08	*0.07*	1
Sponge spicules																						
Sponges from the Rio Negro (unidentified species)																		−0.91	0.07	−0.48	0.06	3

leaching. A third leaching step, similar to the second one, was added to the original procedure of Ragueneau et al. (2005) in order to check that all the BSi had really been dissolved during the first digestion step. In consequence, the Al:Si ratio should then be similar in the second and third leaching solutions. According to Ragueneau et al. (2005) the uncertainty on BSi measurements is ca. 10% but can vary with the importance of the correction. As pointed out in Hughes et al. (2011a) the natural presence of Al in amorphous silica is not taken into account and could therefore induce a small underestimation of the BSi concentration. A few BSi data are missing (see Table 1), two in the tributaries, where the large amount of suspended matter prevented an accurate correction of the LSi contamination, and two at Óbidos where the filters were missing.

Sponges were first rinsed in order to remove lithogenic particles, then heated and sonicated several times in hot concentrated HNO_3 in order to separate spicules from organic matter. After rinsing with de-ionized water (Milli-Q, Milli-Pore), spicules were sieved on a 100 µm filter so that possible remaining fine clays were removed. Spicules were then dried and melted with NaOH at 730 °C in silver crucibles following the method of Georg et al. (2006a) and recovered in de-ionized water. Dissolved samples of spicules were then purified with cation exchange resins following the same method as used for the river water samples (see below).

3.3. Isotopic analyses

The detailed methodology used for samples preparation prior to isotope analyses can be found in Hughes et al. (2011b). The water samples were first treated by photo-ozonolysis following the method described in Hughes et al. (2011b) to mineralize the dissolved organic matter. Cation exchange resins (BioRad's DOWEX 50W-X12) were then used to remove cations from sample solutions following the method described by Georg et al. (2006b). Si isotopes were measured with a Nu Plasma MC-ICP-MS (Nu Instruments) at the Université Libre de Bruxelles, operating in dry plasma mode with a Cetac Aridus II desolvating nebulization system. The mass bias was corrected

through external Mg doping (Cardinal et al., 2003), and the long-term instrumental drift was corrected with the sample-standard bracketing technique relative to the NBS28 silica sand standard (National Institute of Standards and Technology, RM #8546) or an equivalent in-house standard (*Pro Analysi* Quartz from Merck). All results presented in this study are reported relative to NBS28 following:

$$\delta^{X}\mathrm{Si} = (({}^{X}\mathrm{Si}/{}^{28}\mathrm{Si})_{\mathrm{sample}}/({}^{X}\mathrm{Si}/{}^{28}\mathrm{Si})_{\mathrm{NBS28}} - 1) \times 1000 \qquad (1)$$

with ^{X}Si being either ^{29}Si or ^{30}Si. It was recently shown that anionic species, which are not removed by the cation exchange resin, could cause significant matrix effects (van den Boorn et al., 2009; Hughes et al., 2011b). In order to solve this issue, both samples and bracketing standards were doped with acids in large excess compared to the naturally occurring anion concentrations thereby hiding any natural variations of the anion matrix following the method of Hughes et al. (2011b). The acid doped matrix of NO_3^-, Cl^-, SO_4^{2-}, and PO_4^{3-} was adjusted to 3000 mg/L (4.8×10^{-2} N), 100 mg/L (2.8×10^{-3} N), 200 mg/L (4.2×10^{-3} N), and 20 mg/L (6.2×10^{-4} N), respectively. The isobaric interference of $^{14}N^{16}O$ on the ^{30}Si peak is resolved by using the pseudo-high resolution that consists of measuring on the low mass side of the peak, which is free of interference (Abraham et al., 2008). All replicates are total procedural replicates. The accuracy of the δ^{30}Si measurements was checked on a daily basis by measuring a secondary reference material of known isotope composition (Diatomite; Reynolds et al., 2007). The long-term average analytical reproducibility and accuracy on this reference material for δ^{30}Si were of ±0.14‰ ($\pm 2\sigma_{SD}$, $n = 11$). All results of the Si isotope measurements are in agreement with a mass dependent equilibrium fractionation line ($\delta^{30}\mathrm{Si} = 1.93 \times \delta^{29}\mathrm{Si}$).

4. RESULTS

4.1. Dissolved load composition

DSi concentrations in the studied samples range from 47 µmol/L in the upper Rio Negro up to 257 µmol/L in the Rio Branco (Table 1). The low concentrations measured for the upper Rio Negro are less than half those observed in other black rivers in the Congo Basin (Dupré et al., 1996) or in French Guiana (Sondag et al., 2010). At Óbidos, the average DSi concentration during the period studied was 129 ± 19 µmol/L ($\pm 2\sigma_{SD}$). The river cross-section sampled at Óbidos was homogeneous with an average DSi content of 135 ± 2 µmol/L ($\pm 2\sigma_{SD}$; Table 2).

The chemical composition of the rivers results from the contributions of several sources. This includes atmospheric inputs and evaporite rocks which are not involved in the Si cycle; the dissolved load must therefore be corrected for these inputs. Atmospheric inputs are often corrected using normalization to chloride (Stallard and Edmond, 1981): Assuming Cl content in river water originates from the atmosphere and has a conservative behavior we can correct the atmospheric input following $X_{Atm} = Cl_{Riv} \times (X/Cl)_{Mar}$, where Cl_{Riv} is the molar concentration of Cl measured in the river water, X_{Atm} is the amount of an element deriving from atmospheric inputs, and $(X/Cl)_{Mar}$ is the marine ratio of this element relative to Cl. The marine ratio is preferred to rain ratio to avoid taking into account inputs that originate from the basin itself (Gaillardet et al., 1997). However, this correction method is only valid if Cl can be considered as totally derived from marine aerosols. Black and shield rivers are free from significant influence of evaporite rocks (Stallard, 1980; Gaillardet et al., 1997) but some of the Andean rivers drain evaporites, thereby influencing the chemistry of the samples from the Solimões and subsequently from the Amazon at Óbidos. Using the method proposed by Gaillardet et al. (1997) we will assume that Cl concentrations above 20 µmol/L result from evaporite dissolution. After correction for atmospheric inputs, cations were corrected using the average X/Cl ratio from data reported by Stallard (1980) for salt springs and streams with Cl concentrations greater than 1000 µmol/L – indicating an overwhelming influence of evaporites in the chemistry of water – in some Andean drainages; with X/Cl molar ratios of 1.01, 0.02, 0.32 and 0.09 for X being Na, K, Ca and Mg, respectively. Due to the presence of evaporites the correction for Na can reach 60% in the Solimões and Amazon samples. Similarly, the atmospheric correction of the upper Rio Negro is also very significant for Na and Mg (up to 53%) due to its extreme dilution. Finally, note that due to a HCl contamination in the two later samples of the Rio Branco (7/2010 and 10/2010), the Cl concentration of the following month was used as an approximation. The Cl content is very stable during the period following these samplings (12 ± 4 µmol; $\pm 2\sigma$; $n = 10$) and given the

Table 2
DSi concentrations and isotopic signatures measured in the section of the Amazon at Obidos. σ_{SD} on isotopic ratio is given as the standard deviation on the n replicates, most of them are below the long-term analytical reproducibility ($2\sigma_{SD} = 0.15$‰). Measured δ^{30}Si ratios (in ‰) show no variations in the water column, while lateral variations are close to analytical resolution.

Sample	Depth m	Distance from left bank (max. = 2431 m)	DSi µmol/L	δ^{30}Si ‰	$2\sigma_{SD}$	δ^{29}Si ‰	$2\sigma_{SD}$	n
OB 01–04 0 m	0	1601	134	0.71	0.02	0.36	0.04	2
OB 02–07 0 m	0	690	135	0.80	0.19	0.44	0.04	3
OB 03–03 0 m	0	114	137	0.81	0.05	0.43	0.03	2
OB 04–03 0 m	0	1951	135	0.87	0.12	0.44	0.08	3
OB 02–05 6 m	6	690	134	0.79	0.08	0.46	0.08	3
OB 02–04 14 m	14	690	135	0.81	0.03	0.44	0.04	2
OB 02–03 28 m	28	690	134	0.82	0.00	0.44	0.00	2
OB 02–01 56 m	56	690	134	0.81	0.13	0.43	0.04	2

limited impact of the atmospheric correction on these samples a deviation of the Cl concentration within these $\pm 2\sigma$ would only induce an error of 3% on the estimated Si mobility (cf. Section 5.2 discussion on weathering).

4.2. Biogenic Si contents

Twenty samples of suspended matter were analyzed for their BSi content. The BSi measured on the filters range from below detection limit up to 13.4 μmol/L. In the tributaries, the concentrations were especially high in the Solimões (Andean river) where the BSi content can be equivalent to up to 12.5% of the total Si (sum of DSi and BSi). To the opposite, the BSi content measured in shield and black rivers was always very low (less than 4 μmol/L) and never reached more than 1.5% of the total Si content. In the Amazon main stem (Óbidos), the maximum BSi concentration was measured when the discharge was the lowest (12.4 μmol/L in November 2010). This is much lower than the 73.9 ± 17.6 μmol/L ($n = 4$) measured by Conley (1997) in the Amazon. The average BSi concentration at Óbidos was of 9.2 ± 5.1 μmol/L ($\pm 2\sigma_{SD}$, $n = 4$). This is close to the annual average concentration measured in another large tropical river, the Congo River (11.2 ± 3.8 μmol/L; Hughes et al., 2011a). In average, the BSi concentration that we measured in surface water from all rivers represents ca. 3% of the total Si (BSi + DSi).

4.3. Silicon isotopes

At Óbidos, δ^{30}Si ratios measured in surface along the width of the cross-section varied slightly from +0.71‰ up to +0.87‰ with the right bank of the river being more variable (Table 2). However, these variations might not be significant as they are close to our long-term analytical reproducibility (±0.14‰, $\pm 2\sigma_{SD}$). The depth profile was homogeneous with a mean value of $+0.80 \pm 0.01$‰ ($n = 5$) and a standard deviation clearly below our long-term analytical reproducibility. The average δ^{30}Si ratio measured in the whole section was of $+0.80 \pm 0.09$‰ ($\pm 2\sigma_{SD}$; $n = 8$); the standard deviation on all the samples of the section is smaller than our long-term analytical reproducibility.

The δ^{30}Si ratios measured in the DSi in the whole basin ranged from −0.01‰ in the Rio Negro to +2.28‰ in the Rio Solimões. At Óbidos, the seasonal variations of the Amazon signature ranged from +0.71‰ up to +1.76‰ with an average δ^{30}Si ratio of +1.05‰. The δ^{30}Si signature of the DSi exported to the estuary (weighted for DSi flux) for the period considered is +0.92‰. On a δ^{30}Si vs. DSi graph (Fig. 2A), the upper Rio Negro clearly distinguishes itself from the other rivers with both a low DSi concentration and δ^{30}Si ratio. These low values are among the lowest δ^{30}Si ratios ever measured in river waters and are consistent with those observed in other black rivers in the Congo Basin (Cardinal et al., 2010). Among the other samples, the main trend shows an increase of δ^{30}Si signature with increasing DSi concentration ($R^2 = 0.69$, $n = 16$, $p < 0.001$), aligned with the samples of the Rio Negro. This correlation is especially strong in the shield rivers (Rio Branco and Rio Tapajós; $R^2 = 0.91$, $n = 7$, $p < 0.001$). Then, a group of five samples, all from Andean rivers (two from the Rio Solimões, two from the Amazon, and one from the Rio Madeira), define a trend with δ^{30}Si ratios increasing with decreasing DSi concentrations. δ^{30}Si signatures also correlate significantly with cations concentration (corrected for atmospheric and evaporite inputs; Fig. 2B; $R^2 = 0.66$; $p < 0.001$), even though the Andean rivers tend to have a higher cation concentration due to carbonate dissolution. In most rivers, high water periods correspond to low DSi concentrations, high DSi yield and low δ^{30}Si signature. The spicules of the sponges collected in the Rio Negro have an average δ^{30}Si ratio of -0.91 ± 0.07‰ ($\pm 2\sigma_{SD}$,$n = 3$).

5. DISCUSSION

Dissolved Si (DSi) in rivers is nearly always enriched in heavy isotopes relative to the mean value of the continental crust. Hitherto, the reported δ^{30}Si ratios range from −0.1‰ up to +3.4‰ (e.g., De La Rocha et al., 2000; Ding et al., 2004; Alleman et al., 2005; Ziegler et al., 2005a; Georg et al., 2006a, 2007; Cardinal et al., 2010; Engström et al., 2010; Hughes et al., 2012). These positive signatures are thought to result from two main fractionating processes: (1) Biological silica production, which includes uptake by diatoms (De La Rocha et al., 1997) and by higher plants (Opfergelt et al., 2006; Hodson et al., 2008), and (2) Weathering and secondary clay formation (Ziegler et al., 2005a,b; Georg et al., 2007). The respective influences of these fractionating processes will be discussed below.

5.1. River homogeneity and diatom uptake

It has recently been shown that the Rio Solimões at Manacapuru presents significant lateral heterogeneities with regard to its concentration of Na and isotopic composition of Sr (Bouchez et al., 2010). This heterogeneity is attributed to the difficulty of the river to fully mix with its tributaries due to a laminar type of flow; it was therefore important to control the representativeness of our samples. The homogeneity of silicon in the river cross-section at Óbidos and the absence of diatom uptake are attested by the very good homogeneity of both the silicon concentration (135 ± 2 μmol/L, $2\sigma_{SD}$) and the δ^{30}Si ratios ($+0.80 \pm 0.09$‰; $\pm 2\sigma_{SD}$). It is also noteworthy that the average δ^{30}Si signature of the section is close to that measured one week later during the regular monthly sampling (+0.80‰ and +0.87‰, respectively). For these reasons, we can reasonably expect our surface sampling to be representative for the δ^{30}Si signature of the whole river section at Óbidos. However, caution should be taken because the homogeneity has been checked during flood (2nd July 2010), a period that is more likely to be free of any observable influence of diatoms (Istvánovics and Honti, 2011; Hughes et al., 2011a) and might not be representative of rivers during seasonal diatom growth: these algae indeed preferentially incorporate light isotopes when taking up DSi to build their frustules (De La Rocha et al., 1997; Fripiat et al., 2011) and thereby increase the δ^{30}Si ratio of the

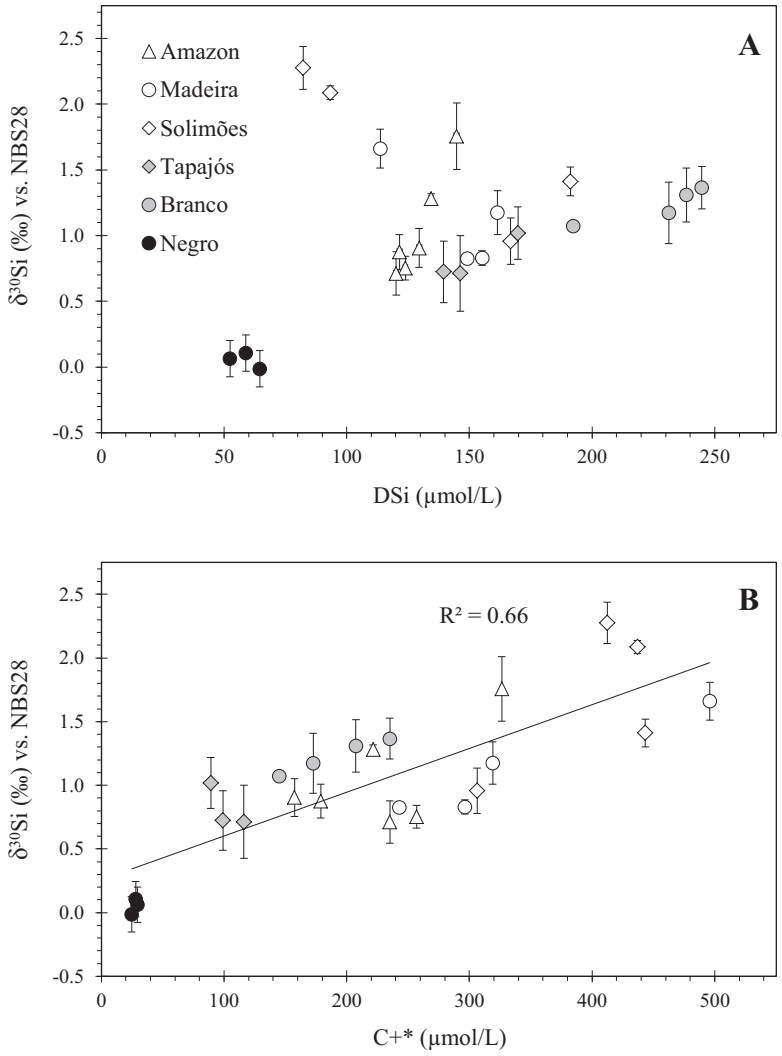

Fig. 2. Evolution of the isotope signature in large rivers of the Amazon Basin (A) with dissolved Si concentration. (B) With the sum of major cations (corrected for atmospheric inputs and evaporite dissolution). Andean rivers are represented by open symbols, shield rivers by shaded symbols and black waters of the Rio Negro by black symbols. Error bars are $2\sigma_{SD}$.

remaining DSi. Given the exceptional depth of the rivers studied here (e.g., more than 60 m in the Amazon and more than 30 m in the Rio Solimões) it is unlikely that the surface samples will remain representative of the whole water column when a marked influence by diatoms is present at the surface, but as no homogeneity study has been conducted during such periods the question will remain open. In shield and black rivers, any impact of diatoms growth on the $\delta^{30}Si$ signatures can probably be ruled out as BSi represents less than 1.5% of the total Si (sum of DSi and BSi). In Andean rivers, as the fraction of BSi in the total Si is higher, a slight influence of diatoms is possible. We however note that the important amount of suspended mater of Andean river is probably not favorable to the development of large diatom blooms and assuming that the measured BSi is representative for the true BSi content, the highest BSi/DSi ratio – occurring during base flow conditions – remains too low to impact the $\delta^{30}Si$ of the dissolved load (maximum increase of +0.15‰ in Solimões 4/2010 based on a fractionation factor of −1.2 for diatom uptake; Fripiat et al., 2011). Moreover, in term of annual average, the contribution of base flow period, when the diatom impact is more important, to the annual flux is limited which also reduces the impact on the $\delta^{30}Si$ annual value. It is however important to keep in mind for the following discussion that the question of the true impact of diatoms on the riverine isotope signatures remain imperfectly constrained and that a significant biological impact cannot totally be ruled out. The relation between BSi content measured in the suspended matter and the impact on $\delta^{30}Si$ signature is not always straightforward (Hughes et al., 2011a). Estimations of diatoms impact on $\delta^{30}Si$ based on measured BSi must therefore be considered cautiously. It is also noticeable that two samples from the Solimões have DSi concentrations below 100 µmol/L, significantly lower than the average concentrations of this river (157 ± 26 µmol/L, $n = 94$; $\pm 2\sigma$; ORE-Hybam database). Whether these low DSi contents must be attributed to a

biological consumption or to secondary mineral formation is unclear.

5.2. Weathering processes

5.2.1. Water geochemistry

Weathering and the subsequent clay formation are known to be important processes driving the riverine $\delta^{30}Si$ signature and it has been proved that it can induce substantial isotope fractionation, e.g., in Swiss and Icelandic catchments where biogenic influence could be excluded (Georg et al., 2006b, 2007). The good correlation observed throughout the Amazon Basin between $\delta^{30}Si$ signature and DSi and C^{+*} concentrations (Fig. 2B) seems to indicate that $\delta^{30}Si$ signatures could be mainly controlled by chemical weathering in the whole basin. However, absolute concentrations are influenced by dilution and evaporation effects. Since elemental ratios are more conservative they are therefore preferable when looking at weathering reactions. Si/Na^* or $Si/(Na + K)^*$ ratios (where $*$ indicate the correction for atmospheric inputs and evaporite dissolution) are commonly used as proxy for the intensity of silicate weathering in the Amazon Basin (Stallard and Edmond, 1987; Edmond et al., 1995). Unlike other major elements that have important carbonate sources, dissolved Na and K originates only from silicate weathering, atmospheric inputs, and evaporite dissolution. After applying a correction for these later sources (cf. Section 4.1), Na^* and K^* are derived solely from silicate rock weathering. As Na and K are generally not incorporated in clays produced during weathering in the Amazonian Basin (Stallard, 1980), they can be considered as a marker of primary silicate weathering. The $Si/(Na + K)^*$ ratio measured in solution will therefore decrease with the proportion of Si remaining immobilized in neoformed minerals. According to Stallard and Edmond (1987), in the Amazon Basin this ratio can be used as an indication on the type of clay formed during the weathering process: a ratio lower than 2 indicates a tendency to form 2:1 clays such as smectites (bisiallitization process; Tardy, 1971), whereas for a ratio from 2 to 3.5 kaolinite neoformation dominates (monosiallitization process). Above 3.5 all the Si is leached and gibbsite is formed (allitization process). These different average ratios depend on the composition of the bedrock. Quartz dissolution and biological uptake, if any, would also influence these ratios. The data are reported in Fig. 3. $Si/(Na + K)^*$ ratios measured are consistent with previous publications and with the mineralogy described for the respective areas: Data from the Rio Negro fall in the monosiallitization area but tend toward allitization, they are also below quartz saturation (100 μmol/L of DSi; Brantley et al., 1986). In shield rivers, the data fall between

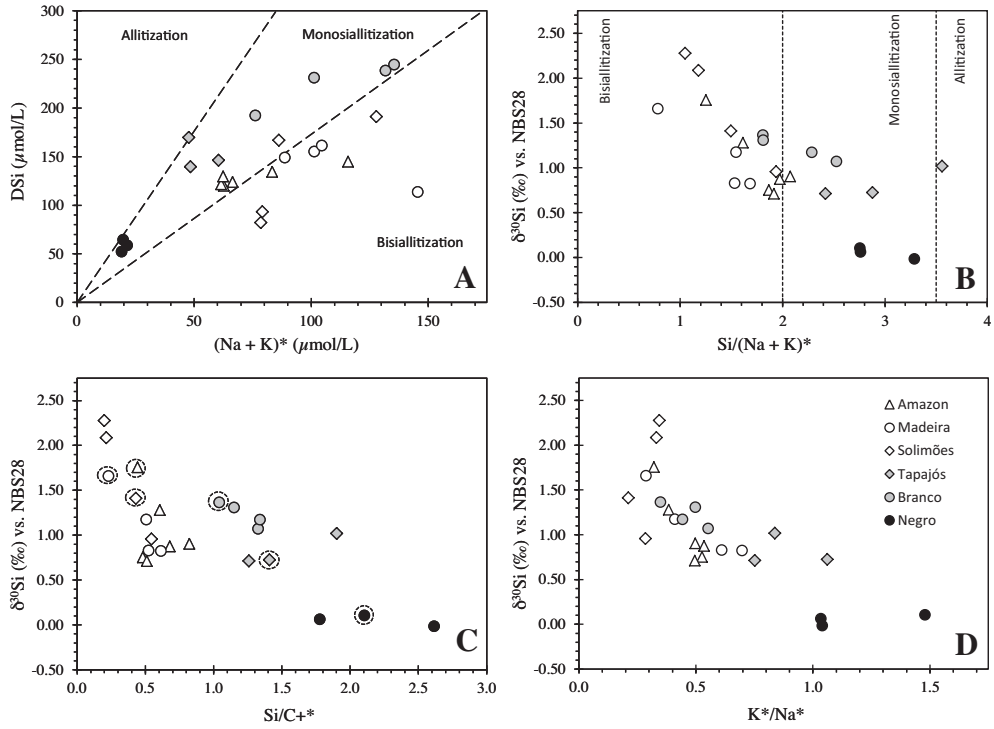

Fig. 3. Plots of DSi (A) and $\delta^{30}Si$ ratio (B,C,D) vs. water geochemistry. The ratio between Si and $(Na + K)^*$ varies depending on the fraction of Si remaining immobilized in neoformed clay minerals and gives an indication on the type of clay formed during the weathering process. The dashed lines indicate the limits between different types of weathering based on the average basement rocks (assuming no dissolution of quartz). Samples within the bisiallitization area tend to form mainly 2:1 clays such as smectites; monosiallitization correspond to a predominant kaolinite formation and during the allitization process all the Si is leached and gibbsite is formed (cf. Section 5.2.1). These different ratios are indicative and depend on the exact composition of the bedrock. Symbols description in D is given for all panels. Circled symbols in figure C correspond to samples with the lowest discharge for each river.

the monosiallitization area and the allitization area, suggesting the preferential formation of kaolinite and gibbsite and the complete leaching of soluble cations. This intense weathering is also consistent with previous conclusions from Edmond et al. (1995) for rivers draining the Guiana Shield. Finally, in the Andean tributaries and in the Amazon at Óbidos most of the samples plot in or close to the bisiallitization area, suggesting the production of both 2:1 clays and kaolinite, which is consistent with previous studies in these rivers (Stallard and Edmond, 1987; Guyot et al., 2007). Note that in the different rivers sampled, the Si concentration tends to increases with $(Na + K)^*$. A trend similar to that observed for $Si/(Na + K)^*$ also exists with Si/C^{+*} (Fig. 3C), which confirms that the heavier $\delta^{30}Si$ signatures of Andean rivers are associated with dissolution of primary cation-rich minerals and probable precipitation of kaolinite-smectite like assemblages. Even though most of the Ca and Mg obviously come from carbonate dissolution in the Andes, the relationship between $\delta^{30}Si$ and Si/C^{+*} observed for Madeira and Solimões rivers ($R^2 = 0.91$; fig. 3C) raises questions about the influence of these Mg and Ca fluxes on the silica cycle; Stallard and Edmond (1987) suggested that in the Andes the high cations concentration rather than the amount of DSi drives the formation of 2:1 clays and that the formation of these clays would in turn limit the DSi concentrations. When compared to $\delta^{30}Si$ signatures, the $Si/(Na + K)^*$ ratios of each river display negative trend, apart from the Tapajós (which nevertheless lies within a broad trend). Fig. 3C show that most rivers are marked by a seasonal effect with higher $Si/(Na + K)^*$ and Si/C^+ at low discharge. The higher release of cations during baseflow is consistent with a higher contribution of primary silicate weathering and deeper origin of water, close to the weathering front.

Apart from the isotope fractionation induced by weathering and clay formation, other processes might also have an influence on the isotope signature. It is well demonstrated that plants enhance chemical weathering (Lucas, 2001; Brantley et al., 2011) and play an important role in soil genesis in the lowland and shield parts of the basin (Lucas et al., 1993). In the Amazonian rainforest, the amount of silica cycled annually through plants not only impacts soil processes, but has also been estimated to be three- to fourfold greater than the Si leached out of the system (Lucas et al., 1993; Lucas, 2001). However, the direct influence of plants on the riverine $\delta^{30}Si$ signature is hard to estimate, especially the impact of phytoliths formation. Phytoliths are known to have light $\delta^{30}Si$ signatures relative to the dissolved Si source (e.g., Ding et al., 2005; Opfergelt et al., 2006), but Opfergelt et al. (2008) suggested that the magnitude of phytoliths impact on river Si isotope signatures would depend on their fate. Indeed, the isotope compositions of rivers would be enriched in heavy isotopes if Si from phytoliths is not recycled (i.e., permanent phytoliths accumulation in soils or export via erosion), but poorly impacted by plant recycling if phytoliths are dissolved in soils. For black and shield rivers, both export via erosion and a significant permanent storage in soil are unlikely given the low erosion rate and the important soil–plant Si fluxes compared to Si export to rivers. The system is therefore expected to be at equilibrium and the phytolith pool can reasonably be assumed to be a simple transfer reservoir with no significant impact on the isotope signature of the DSi released to streams, at least on an annual scale. Seasonal imbalances between the silicon uptake by plants and the dissolution of phytoliths are possible and could influence the isotope signature of the DSi in rivers, but if phytoliths can be considered as a simple transfer reservoir on an annual scale, their average signature should be similar to that of DSi released by weathering reactions, thereby limiting the impact on seasonal variations. In Andean regions, the high weathering fluxes and DSi yields along with the scarcer vegetation are likely to limit the impact of plants on the Si cycle.

In order to test a possible impact of vegetation, it is also possible to consider the K^*/Na^* ratio in water. Contrary to Na^*, K^* may be recycled in clays and be involved in the soil–plant cycle as macro-nutrient. In the latter case, a higher K^*/Na^* ratio may therefore correspond to a superficial origin of water with partial contribution of elements involved in plant cycle. The data are presented in Fig. 3D and a trend is visible at the basin scale between the K^*/Na^* ratio and the $\delta^{30}Si$ signature ($R^2 = 0.61$). At the sub-basin scale, a correlation only appears for the Rio Madeira ($R^2 = 0.91$). However several authors (e.g., Stallard, 1980; Edmond et al., 1995; Tardy et al., 2005) have observed that in the Andean rivers and soil solutions K concentrations are controlled mainly by weathering reactions while it indeed reflect biological cycling in some other (e.g., Rio Negro). The K/Na ratio in Andean rivers is lower than what would be expected if bedrock weathered completely (ca. 0.55 for acid rocks), this presumably reflects a greater resistance of K-feldspar and micas to chemical breakdown (Stallard and Edmond, 1983). The K/Na ratio is higher in shield rivers and black waters where it likely reflects the more efficient breakdown of primary minerals and thus the more complete leaching of K into solution. The trend observed at the basin scale therefore seems to be more an indirect correlation of the $\delta^{30}Si$ signature with the weathering type than a tracer to distinguish water from superficial origin from baseflow or a tracer of the recycling by vegetation. So although there are good arguments to assume that the direct effect of plants on rivers isotope composition is limited, their potential effect can never totally be ruled out and should be kept in mind during the following discussion.

Following our observations on Fig. 3, we will now use elemental ratios to estimate the relative mobility of Si, which is the fraction of the Si initially released by the weathering of primary minerals that is not subsequently incorporated in neoformed minerals. This can be achieved by comparing the ratio between Si and reference elements in water to that same ratio in the parent rock following:

$$f_{Si} = [Si/(Na + K)^*]_{Riv}/[Si/(Na + K)]_{Rock} \quad (2)$$

where f_{Si} is the mobility of Si, $[Si/(Na + K)^*]_{Riv}$ is the molar ratio of the riverine dissolved load and $[Si/(Na + K)]_{Rock}$ the molar ratio for average acidic rocks (ignoring normative quartz; Stallard, 1980; Edmond et al., 1995). Note that the average $Si/(Na + K)$ ratio from acidic rock will be used

for all rivers even though marine sediments are a significant part of the bedrock in the Andes (especially the Madeira Basin). As the average Si/(Na + K)* ratio from shales is close to that of acidic rock (3.66 and 3.53, respectively; Stallard, 1980) this simplification does not significantly affect the final results. In the Rio Madeira, the f_{Si} could however be slightly overestimated due to the retention of K in chemically resistant potassium-bearing mica that are abundant in this basin (Stallard, 1980). The $\delta^{30}Si$ signature will decrease with increasing f_{Si}: A f_{Si} of 1 corresponds to a congruent dissolution of the rock regarding Si; no Si is incorporated in secondary minerals and the riverine $\delta^{30}Si$ signature consequently corresponds to that of the primary Si source. This $\delta^{30}Si$ signature of unweathered igneous rocks in the Amazon Basin can be estimated based on their Si content. Savage et al. (2012) showed that for igneous rocks the Si isotope signature correlates with the percentage of SiO_2. According to Stallard (1980), this percentage is 59% for the shields, which should correspond to a $\delta^{30}Si$ ratio of ca. −0.24‰ – close to the average signature of granite (−0.23‰ ± 0.15; ±2σ) reported by Savage et al. (2012). Igneous rocks throughout the Andes also have an acid to intermediate composition with a similar average Si content (Stallard, 1980). Sedimentary rock mostly cover a similar range of isotope ratios even though they can sometimes reach much lower signature (Douthitt, 1982; Ding et al., 1996; Savage et al., 2012, 2013). Variations between these primary Si sources are therefore generally small and it is unlikely that the geological substrate can generate important variations in the isotope composition of rivers. An average $\delta^{30}Si$ signature of ca. −0.24‰ seems to be a good approximation even though the presence of sedimentary rocks in the Andes render the exact average $\delta^{30}Si$ signature of Andean primary Si source less certain. Using f_{Si} as a tracer of Si mobility, Fig. 4A shows it has a net global negative correlation with $\delta^{30}Si$ signatures ($R^2 = 0.54$; $p < 0.001$) and each river, apart from Tapajós, display lower $\delta^{30}Si$ signatures with increasing Si mobility, which is consistent with the dependence of Si isotope ratio to the clay formation regime. Although all rivers fit on a global trend, the three types of rivers tend to form sub-clusters and will therefore be analyzed separately in the following sections.

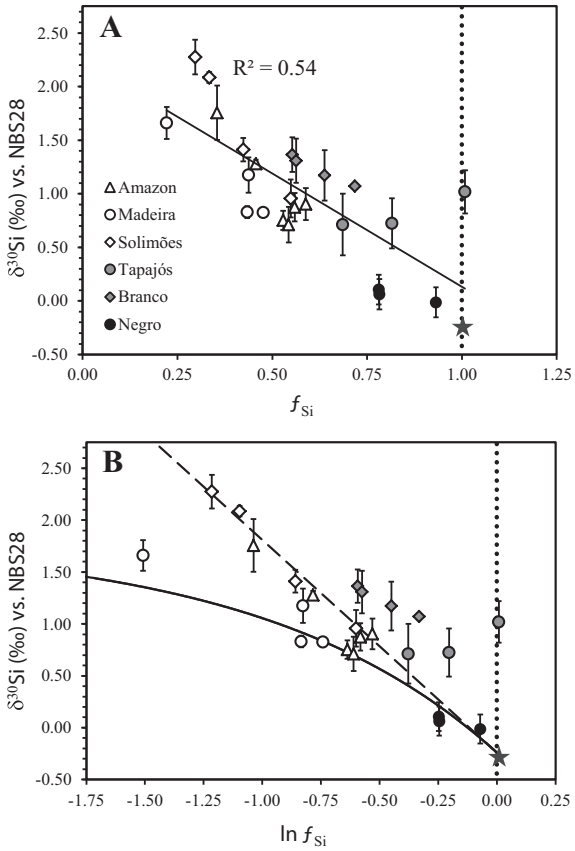

Fig. 4. Evolution of the isotope signatures in large rivers of the Amazon Basin as a function of the estimated Si mobility (A). The stars indicate the estimated rock end-member. If the fractionation follow a Rayleigh model, then in a $\delta^{30}Si$ vs. ln(f_{Si}) space (B) the slope will give an estimation of the fractionation factor. The Solimões data follow a linear trend (dashed line) corresponding to a Rayleigh type fractionation, with a slope of −2.05. The evolution of the isotope signature following a batch equilibrium model using this same fractionation factor is also indicated (solid line). Error bars are $2\sigma_{SD}$.

5.2.2. Black rivers

The very low $\delta^{30}Si$ signatures in the upper Rio Negro (+0.05 ± 0.06‰) are similar to those measured by Cardinal et al. (2010) in the black rivers of the Congo Basin, despite the lower DSi concentrations observed in the Rio Negro (161 μmol/L and 59 μmol/L in average, respectively). Such an unusually low $\delta^{30}Si$ signature, slightly enriched compared to the estimated signature of the bedrock (−0.24‰) is consistent with the high f_{Si} and can be explained by the high weathering intensity in this basin. It results in two processes that can occur simultaneously and that are both likely to set the riverine $\delta^{30}Si$ ratios to values close to that of the primary Si reservoir. DSi can either derive from the congruent dissolution of material, which means that fractionation processes occurring during the dissolution are extremely limited, or be the result of a mixing between two DSi sources with opposite signatures. This latter hypothesis was favored by Cardinal et al. (2010) in the Congo Basin: They suggested a mixing between DSi with low $\delta^{30}Si$ ratio, originating from the enhanced dissolution of neoformed clay due to the high humic acids content (Lucas et al., 1993; Chauvel et al., 1996), and DSi with high $\delta^{30}Si$ ratio released in deeper horizons, at the weathering front, where clay formation occurs and enriches DSi in ^{30}Si. Such balance in the formation and destruction of clay is especially likely to take place in the upper Rio Negro given its highly transport-limited regime, preventing fractionated material to be exported before it got dissolved. The congruent dissolution of primary material is the second source of DSi with $\delta^{30}Si$ signatures similar to that of the bedrock. It can result from the direct allitization of primary aluminosilicate minerals into gibbsite as this mineral is known to form abundantly in the upper Rio Negro Basin (Lucas, 2001; Fritsch et al., 2009). As gibbsite does not contain Si, the process can be compared to a congruent dissolution for Si and hence result in the absence of net Si isotope

fractionation. Both the formation of gibbsite and the formation-destruction of clays are supported by the high f_{Si} values (Fig. 4A) that reflect the high mobility of Si. In addition, congruent dissolution of quartz may also take place given the important fraction of quartz present in the podzolic soils drained by the Rio Negro and given that – unlike black rivers of the Congo Basin – the Rio Negro is undersaturated with respect to quartz (below 100 μmol/L). Based on previous researches on isotopes of other elements (Sr and Li) during mineral dissolution, Basile-Doelsch et al. (2005, sup. mat.) suggest that there should be no Si isotopes fractionation during the dissolution of quartz minerals, which could therefore be a source of DSi with a low $\delta^{30}Si$ signature. However, due to the low residence time of the percolating water in the podzol areas (Lucas et al., 1996), quartz dissolution is likely to only account for a minor part of the DSi.

We can further add that Chauvel et al. (1996) pointed out the presence of a particularly important amount of siliceous sponge spicules in the sediments of some tributaries of the Rio Negro. The flux of DSi taken up by sponges in continental environment remains so far unstudied and no data exists on the BSi production by sponges in the Rio Negro or the Amazon. $\delta^{30}Si$ ratios in siliceous sponges have been reported only for marine species and are among the most negative ever measured (from $-4.13‰$ to $+0.87‰$; Douthitt, 1982; De La Rocha, 2003; Hendry et al., 2010; Wille et al., 2010). Given the negative signature observed in our sponge samples ($-0.91 \pm 0.3‰$, Table 1), siliceous sponges might have an impact on the signature of the river, although it is certainly limited as the $\delta^{30}Si$ signature of the DSi is already very low. It is probable that the amount of DSi fixed in sponges remains low in comparison with the total DSi flux. Alternatively, sponge spicules could represent just a transfer reservoir – a large fraction of it being dissolved – and thereby have a neutral impact on the $\delta^{30}Si$ signature of the river.

5.2.3. Andean rivers

Andean rivers are in many ways opposite to black rivers: they correspond to weathering-limited conditions and have high dissolved elements concentrations. They also have much higher $\delta^{30}Si$ signatures, which globally decrease with relative DSi mobility (Fig. 4A). As shown by Georg et al. (2007), the relation between f_{Si} and $\delta^{30}Si$ can be described following either a batch equilibrium or a Rayleigh-type model:

Rayleigh :

$$\delta^{30}Si = \delta^{30}Si_0 + \varepsilon(\ln f_{Si}) \quad (3)$$

$$\delta^{30}Si_p = \delta^{30}Si + \varepsilon \quad (4)$$

Batch equilibrium :

$$\delta^{30}Si = \delta^{30}Si_0 - \varepsilon(1 - f_{Si}) \quad (5)$$

$$\delta^{30}Si_p = \delta^{30}Si_0 + \varepsilon(f_{Si}) \quad (6)$$

where ε is the fractionation factor in permil unit and $\delta^{30}Si$, $\delta^{30}Si_0$ and $\delta^{30}Si_p$ are the isotope compositions of the dissolved silicon, of the unweathered bedrock and of the product, respectively. Like Icelandic rivers (Georg et al., 2007), Andean rivers fit on two different trends. Data from the Rio Solimões follow a Rayleigh type fractionation; in a $\delta^{30}Si$ vs. $\ln(f_{Si})$ space (Fig. 4B), the slopes should provide an estimate of the associated fractionation factor, which corresponds here to $\varepsilon = -2.05 \pm 0.08‰$ ($R^2 = 0.98$; $p < 0.001$) – assuming a primary reservoir with a $\delta^{30}Si$ signature of $-0.24‰$. Most data points from the Amazon at Óbidos also fall on this line. Data from the Rio Madeira on the other hand seem to follow a different trend. The origin of this distinction between the two Andean tributaries can be explained in different ways. It could result either from a different fractionation model or from a much smaller fractionation factor during weathering reactions. Using the fractionation factor of $-2.05‰$ to draw the evolution of DSi signature in a batch equilibrium system we see that it could fit with the data from the Rio Madeira (Fig. 4B) especially when considering the potential overestimation of the f_{Si} mentioned above for this basin. The cause of this difference of fractionation model remains poorly understood, even though it has also been observed on Icelandic rivers (Georg et al., 2007), and would require further studies. One reason that could explain this difference of fractionation type (Rayleigh vs. batch equilibrium) between the Solimões and the Madeira rivers is the massive abundance of mica in the latter that could result in different weathering mechanisms and reaction rates more favorable to a batch equilibrium fractionation (Malmström and Banwart, 1997). Another hypothesis is that data from the Rio Madeira follow a Rayleigh system with a $\varepsilon \approx -1‰$ (not shown). This hypothesis seems less likely as no major difference in the type of clay formed seems able to justify such a difference, but the limited amount of data does not allow to discard it. It could also result from a biological uptake of DSi. Note that unlike in the other Andean rivers, the Madeira sample with the highest $\delta^{30}Si$ signature corresponds to a period of markedly low DSi flux; its higher signature therefore probably has a negligible influence on that of the weighted annual DSi flux. Among the samples from the Amazon Through, the two samples with the highest $\delta^{30}Si$ signatures fall close to the Rayleigh type trend of the Rio Solimões; this is not surprising as these correspond to low flow period when the inputs of the Rio Solimões are proportionally more important.

The fractionation factor of $-2.05‰$ found for the Solimões and the Amazon – and possibly for the Madeira Basin – is similar to that found by Ziegler et al. (2005b) but larger than the $\varepsilon = -1.6‰$ estimated by theoretical calculations for the equilibrium isotope fractionation between kaolinite and quartz (at 20 °C; Méheut et al., 2007) and than that estimated by Georg et al. (2007) for clay formation in basaltic catchments in Iceland ($\varepsilon = -1.5‰$). The variation of the fractionation factor following the type of secondary clay formed remains barely studied, but it has been suggested that neoformed smectites are less fractionated than kaolinite (Georg et al., 2009; Opfergelt et al., 2012) and previously published $\delta^{30}Si$ ratios indeed tend to be more negative in kaolinite ($-1.89 \pm 0.89‰$; $n = 23$) than those measured in smectite ($-0.31 \pm 0.16‰$; $n = 8$; Douthitt, 1982; Ding et al., 1996; Ziegler et al., 2005b; Georg et al., 2009). However, the fact that we find a fractionation factor of $-2.05‰$

in rivers that contain mainly 2:1 clays (ca. 80%; Guyot et al., 2007) suggests a fractionation factor slightly larger for 2:1 clays than for kaolinite – or at least does not support the idea of a smaller fractionation factor. We suggest that the higher δ^{30}Si ratios measured in smectites in other studies could rather result from a lower f_{Si} (i.e. higher fraction of Si incorporated into secondary mineral) rather than a lower fractionation factor. This can be explained based on Eqs. (3–6) through which we see that for a given ε the δ^{30}Si signature of the accumulated product tends to increase with decreasing f_{Si} (Fig. 5).

5.2.4. Shield rivers

Shield rivers present transport-limited conditions in which the physical products of weathering have a longer time to react with soil and ground waters; the erosion rate is also extremely slow (~10 m/10^6 y, Edmond et al., 1995) and results in very thick soils. Using the same method based on $(Na + K)^*$ as reference elements to estimate the mobility of Si, we see that the f_{Si} presents a higher average than Andean rivers (respectively $+0.71 \pm 0.32$ and $+0.44 \pm 0.22$; $\pm 2\sigma_{SD}$; fig. 4). Differences also appear between the Tapajós and the Branco rivers: In the Branco the δ^{30}Si signatures increase with the decreasing $f_{Si,}$ like in Andean rivers ($R^2 = 0.97$; $p < 0.02$) while in the Tapajós the pattern is less clear and tends to follow the opposite trend. For the Rio Branco, the linear regression from the data in Fig. 4B crosses the Y-axis at $+0.82 \pm 0.24‰$. Although this value should be considered cautiously as the error bars are large, a primary source of Si with such a high δ^{30}Si signature is incompatible with the crustal rocks drained. Aside from possible seasonal imbalance in phytoliths formation and dissolution (cf. Section 5.2.1) a bias of the f_{Si} can occur if a significant proportion of DSi is derived from quartz dissolution. Quartz dissolution in shield regions of the Amazon Basin is indeed a well-documented process. Numerous cavities of dissolution have been observed on quartz grains in soils and in the sediments of river shores (e.g., Stallard and Edmond, 1987; Chauvel et al., 1996; Lucas et al., 1996; Dubroeucq and Volkoff, 1998; Lucas, 2001) and Edmond et al. (1995) suggested that quartz dissolution could represent a significant source of DSi in rivers draining shield. This phenomenon is explained by Lucas (2001) as a result of the slow percolation through these thick (20–30 m) and highly weathered soils containing mainly residual quartz and secondary minerals. From the Fig. 4B we see that the samples from the Rio Branco with the highest cation content – where the DSi inputs from quartz dissolution is probably proportionally least – tend toward the trend drawn by the Solimões. This suggests that the isotope fractionation follows a Rayleigh model like in the Solimões. Regarding the Tapajós, the signal is more complex to interpret. From Fig. 4B it seems to be halfway between the Andean rivers trend (no quartz dissolution) and the Rio Branco. Note that for both rivers the DSi flux is ca. one order of magnitude higher during the period of higher f_{Si}, which would correspond to higher inputs from quartz dissolution. The most likely explanation would be that different types of solute end-members are mobilized at low and high discharge flow. An important Si input from quartz dissolution would also explain why one of the Tapajós sample fall on the allitization area (Fig. 3) while still having a heavy δ^{30}Si signature. However, the amount of data for this river is too limited to make more detailed hypothesis.

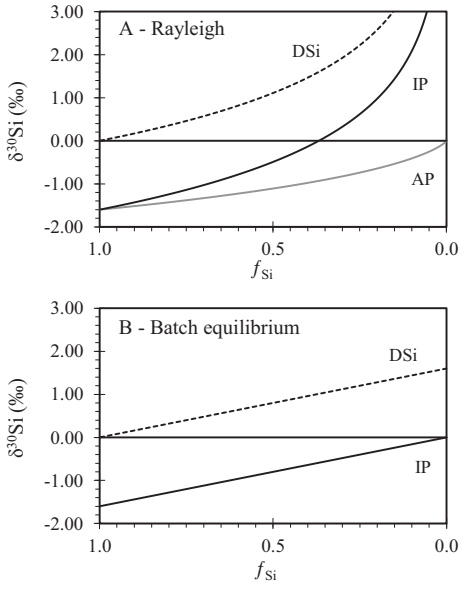

Fig. 5. Evolution of the δ^{30}Si ratio of the different reservoirs following (A) a Rayleigh type fractionation model and (B) a steady-state fractionation model, here for a $^{30}\varepsilon$ of $-1.6‰$. Evolution of the δ^{30}Si ratio of the DSi (solid line), the instantaneous product (IP; dotted line) and the accumulated product (AP; grey line). The IP and AP lines show that different secondary minerals (e.g., kaolinite and smectite) can present different δ^{30}Si ratios if they are formed in different contexts (i.e., different f_{DSi}) without necessarily involving different fractionation factors.

6. CONCLUSIONS

In this study, we reported the first dataset of riverine δ^{30}Si signatures in the Amazon Basin, the largest watershed in the world. Different types of rivers with contrasted chemical and physical characteristics were studied (black, Andean and shield rivers). The data reported here seem to be mainly free of direct biological impact. Based on our results, apart from biological impact, three main factors are likely to influence the riverine δ^{30}Si signatures in the Amazon Basin. A fractionation factor of $-2.05‰$ is observed in Andean rivers and probably reflect the formation of 2:1 clays. The determination of ε for different types of clays is essential and should be an important focus of future researches on silicon isotopes. The second factor is the fractionation model followed in the different basins. The Rio Solimões clearly follows a Rayleigh fractionation model, while the Rio Madeira seems to follow a batch equilibrium model. The cause of this difference could be linked to the different mineralogy in this basin but remains unclear. The third factor is the fraction of DSi incorporated in neoformed minerals. We showed the clear relation between δ^{30}Si signatures and Si mobility in the Amazon Basin. In shield rivers the relation was less direct due to the intense weathering causing important amount of quartz to dis-

solves, but beside this specific case, our results shows that $\delta^{30}Si$ signatures can be a good proxy for Si mobility and thereby for clay formation.

ACKNOWLEDGMENTS

The ORE-HYBAM Observatory is funded by the French Institut de Recherche pour le Développement (IRD), the French Institut des Sciences de l'Univers (INSU) and the Observatoire Midi-Pyrénée (OMP). This work has been supported by the Belgian Federal Science Policy Office (BELSPO) under the contracts Interuniversity Attraction Pole IAP 6/13, CLANIMAE SD/BD/03B, COBAFISH SD/AR/05A and Fleuve Congo (Action 1 and PADD project). T. Rousseau and P. Seyler (IRD) are warmly thanked for providing the section samples and help to collect the sponge samples. We also thank J. de Jong and N. Mattielli (Université Libre de Bruxelles) for the management of the NuPlasma facility, which has been funded by the Fond de la Recherche Scientifique (FRFC 2.4.512.00F). J. Navez and L. Monin (Royal Museum for Central Africa) and A. Silinski (UA) provided valuable help. B. Georg and E. Tipper are thanked for their constructive reviews, as well as a third anonymous reviewer and the AE who significantly helped improving this article.

REFERENCES

Aalto R., Dunne T. and Guyot J.-L. (2006) Geomorphic controls on Andean denudation rates. *J. Geol.* **114**, 85–99.

Abraham K., Opfergelt S., Fripiat F., Cavagna A., de Jong J., Foley S., André L. and Cardinal D. (2008) ^{30}Si and ^{29}Si determinations on USGS BHVO-1 and BHVO-2 reference materials with a new configuration on a Nu plasma multi-collector ICP-MS. *Geostand. Geoanal. Res.* **32**, 193–202.

Alleman L. Y., Cardinal D., Cocquyt C., Plisnier P.-D., Descy J. P., Kimirei I., Sinyinza D. and André L. (2005) Silicon isotopic fractionation in Lake Tanganyika and its main tributaries. *J. Great Lakes Res.* **31**, 509–519.

Alsdorf D., Han S.-C., Bates P. and Melack J. M. (2010) Seasonal water storage on the Amazon floodplain measured from satellites. *Remote Sens. Environ.* **114**, 2448–2456.

Amiotte-Suchet P., Probst J.-L. and Ludwig W. (2003) Worldwide distribution of continental rock lithology: implications for the atmospheric/soil CO_2 uptake by continental weathering and alkalinity river transport to the oceans. *Global Biogeochem. Cycles* **1**, 1038–1051.

Basile-Doelsch I., Meunier J.-D. and Parron C. (2005) Another continental pool in the terrestrial silicon cycle. *Nature* **433**, 399–402.

Berner R., Lasaga A. and Garrels R. (1983) The carbonate-silicate geochemical cycle and its effect on atmospheric carbon dioxide over the past 100 million years. *Am. J. Sci.* **283**, 641–683.

Beusen A., Bouwman A., Dürr H., Dekkers A. and Hartmann J. (2009) Global patterns of dissolved silica export to the coastal zone: results from a spatially explicit global model. *Global Biogeochem. Cycles* **23**, GB0A02.

Bluth G. and Kump L. (1994) Lithologic and climatologic controls of river chemistry. *Geochim. Cosmochim. Acta* **58**, 2341–2359.

Bouchez J., Lajeunesse E., Gaillardet J., France-Lanord C., Dutra-Maia P. and Maurice L. (2010) Turbulent mixing in the Amazon River: the isotopic memory of confluences. *Earth Planet. Sci. Lett.* **290**, 37–43.

Brantley S. L., Megonigal J. P., Scatena F. N., Balogh-Brunstad Z., Barnes R. T., Bruns M. A., Van Cappellen P., Dontsova K., Hartnett H. E., Hartshorn A. S., Heimsath A., Herndon E., Jin L., Keller C. K., Leake J. R., Mcdowell W. H., Meinzer F. C., Mozdzer T. J., Petsch S., Pett-Ridge J., Pregitzer K. S., Raymond P. A., Riebe C. S., Shumaker K., Sutton-Grier A., Walter R. and Yoo K. (2011) Twelve testable hypotheses on the geobiology of weathering. *Geobiology* **9**, 140–165.

Brantley S. L., Crane S. R., Crerar D. A., Hellmann R. and Stallard R. (1986) Dissolution at dislocation etch pits in quartz. *Geochim. Cosmochim. Acta* **50**, 2349–2361.

Callède J., Cochonneau G., Ronchail J., Vieira Alves. F., Guyot J.-L., Guimaraes V. and De Oliveira E. (2010) Les apports en eau de l'Amazone à l'Océan Atlantique. *Rev. Sci. Eau – J. Water Sci.* **23**, 247–273.

Cardinal D., Alleman L., de Jong J., Ziegler K. and André L. (2003) Isotopic composition of silicon measured by multicollector plasma source mass spectrometry in dry plasma mode. *J. Anal. At. Spectrom.* **18**, 213–218.

Cardinal D., Gaillardet J., Hughes H. J., Opfergelt S. and André L. (2010) Contrasting silicon isotope signatures in rivers from the Congo Basin and the specific behaviour of organic-rich waters. *Geophys. Res. Lett.* **37**, L12403.

Chauvel A., Walker I. and Lucas Y. (1996) Sedimentation and pedogenesis in a Central Amazonian Black water basin. *Biogeochemistry* **33**, 77–95.

Conley D. J. (1997) Riverine contribution of biogenic silica to the oceanic silica budget. *Limnol. Oceanogr.* **42**, 774–777.

De La Rocha C. L. (2003) Silicon isotope fractionation by marine sponges and the reconstruction of the silicon isotope composition of ancient deep water. *Geology* **31**, 423–426.

De La Rocha C. L., Brzezinski M. A. and DeNiro M. J. (1997) Fractionation of silicon isotopes by marine diatoms during biogenic silica formation. *Geochim. Cosmochim. Acta* **61**, 5051–5056.

De La Rocha C. L., Brzezinski M. A. and DeNiro M. J. (2000) A first look at the distribution of the stable isotopes of silicon in natural waters. *Geochim. Cosmochim. Acta* **64**, 2467–2477.

Delvaux C., Cardinal D., Carbonnel V. Chou L., Hughes H. J. and André L. (in press) Controls on riverine $\delta^{30}Si$ signatures in a temperate watershed under high anthropogenic pressure (Scheldt – Belgium). *J. Marine Syst.*

Ding T., Jiang S., Wan D., Li Y., Li J., Song H., Liu Z. and Yao X. (1996) *Silicon Isotope Geochemistry*. Geological Publishing House, Bejing.

Ding T., Wan D., Wang C. and Zhang F. (2004) Silicon isotope compositions of dissolved and suspended matter in the Yangtze. *Geochim. Cosmochim. Acta* **68**, 205–216.

Ding T., Ma G., Shui M., Wan D. and Li R. (2005) Silicon isotope study on rice plants from the Zhejiang province, China. *Chem. Geol.* **218**, 41–50.

Douthitt C. (1982) The geochemistry of the stable isotopes of silicon. *Geochim. Cosmochim. Acta* **46**, 1449–1458.

Dubroeucq D. and Volkoff B. (1998) From Oxisols to Spodosols and Histosols: evolution of the soil mantles in the Rio Negro basin (Amazonia). *Catena* **32**, 245–280.

Dupré B., Gaillardet J., Rousseau D. and Allègre C. (1996) Major and trace elements of river-borne material: the Congo Basin. *Geochim. Cosmochim. Acta* **60**, 1301–1321.

Edmond J. M., Palmer M. R., Measures C. I., Grant B. and Stallard R. F. (1995) The fluvial geochemistry and denudation rate of the Guayana Shield in Venezuela, Colombia, and Brazil. *Geochim. Cosmochim. Acta* **59**, 3301–3325.

Engström E., Rodushkin I., Ingri J., Baxter D., Ecke F., Österlund H. and Öhlander B. (2010) Temporal isotopic variations of dissolved silicon in a pristine boreal river. *Chem. Geol.* **271**, 142–152.

Fripiat F., Cavagna A.-J., Savoye N., Dehairs F., Andre L. and Cardinal D. (2011) Isotopic constraints on the Si-biogeochem-

ical cycle of the Antarctic Zone in the Kerguelen area (KEOPS). *Mar. Chem.* **123**, 11–22.

Fritsch E., Allard T., Benedetti M., Bardy M., do Nascimento N., Li Y. and Calas G. (2009) Organic complexation and translocation of ferric iron in podzols of the Negro River watershed. Separation of secondary Fe species from Al species. *Geochim. Cosmochim. Acta* **73**, 1813–1825.

Gaillardet J., Dupré B., Allègre C. J. and Négrel P. (1997) Chemical and physical denudation in the Amazon River Basin. *Chem. Geol.* **142**, 141–173.

Garnier J., Beusen A., Thieu V., Billen G. and Bouwman L. (2010) N:P:Si nutrient export ratios and ecological consequences in coastal seas evaluated by the ICEP approach. *Global Biogeochem. Cycles* **24**, GB0A05.

Georg R. B., Reynolds B. C., Frank M. and Halliday A. N. (2006a) Mechanisms controlling the silicon isotopic compositions of river waters. *Earth Planet. Sci. Lett.* **249**, 290–306.

Georg R. B., Reynolds B. C., Frank M. and Halliday A. N. (2006b) New sample preparation techniques for the determination of Si isotopic compositions using MC-ICPMS. *Chem. Geol.* **235**, 95–104.

Georg R. B., Reynolds B. C., West A. J., Burton K. W. and Halliday A. N. (2007) Silicon isotope variations accompanying basalt weathering in Iceland. *Earth Planet. Sci. Lett.* **261**, 476–490.

Georg R. B., Zhu C., Reynolds B. C. and Halliday A. N. (2009) Stable silicon isotopes of groundwater, feldspars, and clay coatings in the Navajo Sandstone aquifer, Black Mesa, Arizona, USA. *Geochim. Cosmochim. Acta* **73**, 2229–2241.

Guyot J., Jouanneau J. M., Soares L., Boaventura G. R., Maillet N. and Lagane C. (2007) Clay mineral composition of river sediments in the Amazon Basin. *Catena* **71**, 340–356.

Hendry K., Georg R., Rickaby R., Robinson L. and Halliday A. (2010) Deep ocean nutrients during the Last Glacial Maximum deduced from sponge silicon isotopic compositions. *Earth Planet. Sci. Lett.* **292**, 290–300.

Hodson M. J., Parker A. G., Leng M. J. and Sloane H. J. (2008) Silicon, oxygen and carbon isotope composition of wheat (*Triticum aestivum* L.) phytoliths: implications for palaeoecology and archaeology. *J. Quaternary Sci.* **23**, 331–339.

Hughes H. J., Sondag F., Cocquyt C., Laraque A., Pandi A., André L. and Cardinal D. (2011a) Effect of seasonal biogenic silica variations on dissolved silicon fluxes and isotopic signatures in the Congo River. *Limnol. Oceanogr.* **56**, 551–561.

Hughes H. J., Delvigne C., Korntheuer M., de Jong J., André L. and Cardinal D. (2011b) Controlling the mass bias introduced by anionic and organic matrices in silicon isotopic measurements by MC-ICP-MS. *J. Anal. At. Spectrom.* **26**, 1892–1896.

Hughes H. J., Bouillon S., André L. and Cardinal D. (2012) The effects of weathering variability and anthropogenic pressures upon silicon cycling in an intertropical watershed (Tana River, Kenya). *Chem. Geol.* **308–309**, 18–25.

Istvánovics V. and Honti M. (2011) Phytoplankton growth in three rivers: the role of meroplankton and the benthic retention hypothesis. *Limnol. Oceanogr.* **56**, 1439–1452.

Jennerjahn T. C., Knoppers B. A., De Souza W. F. L., Brunskill G. J., Silva E. I. L. and Adi S. (2006) Factors controlling dissolved silica in tropical rivers. In *The Silicon Cycle: Human Perturbations and Impacts on Aquatic Systems*, Scope 66 (eds. V. Ittekkot, D. Unger, C. Humborg and N. T. An). Island Press, pp. 29–51.

Lucas Y. (2001) The role of plants in controlling rates and products of weathering: importance of biological pumping. *Annu. Rev. Earth Planet. Sci.* **29**, 135–163.

Lucas Y., Luizao F., Chauvel A., Rouiller J. and Nahon D. (1993) The relation between biological activity of the rain forest and mineral composition of soils. *Science* **260**, 521–523.

Lucas Y., Nahon D., Cornu S. and Eyrolle F. (1996) Genèse et fonctionnement des sols en milieu équatorial. Comptes rendus de l'Académie des sciences. Série 2. *Sci. Terre Planetes* **322**, 1–16.

Malmström M. and Banwart S. (1997) Biotite dissolution at 25 °C: the pH dependence of dissolution rate and stoichiometry. *Geochim. Cosmochim. Acta* **61**, 2779–2799.

Martinez J. M., Guyot J.-L., Filizola N. and Sondag F. (2009) Increase in suspended sediment yield of the Amazon River assessed by monitoring network and satellite data. *Catena* **79**, 257–264.

Méheut M., Lazzeri M., Balan E. and Mauri F. (2007) Equilibrium isotopic fractionation in the kaolinite, quartz, water system: Prediction from first-principles density-functional theory. *Geochim. Cosmochim. Acta* **71**, 3170–3181.

Mertes L. and Dunne T. (2007) Large rivers: geomorphology and management, effects of tectonism, climate change, and sea-level change on the form and behaviour of the modern Amazon river and its floodplain. In *Large Rivers, Geomorphology and Management* (ed. A. Gupta). John Wiley & Sons Ltd, Chichester, England, pp. 115–144.

Milliman J. (2001) River Inputs. In *Encyclopedia of Ocean Sciences* (ed. J. H. Steele). Academic Press, pp. 2419–2427.

Moquet J.-S., Crave A., Viers J., Seyler P., Armijos E., Bourrel L., Chavarri E., Lagane C., Laraque A., Casimiro W. S. L., Pombosa R., Noriega L., Vera A. and Guyot J.-L. (2011) Chemical weathering and atmospheric/soil CO_2 uptake in the Andean and Foreland Amazon basins. *Chem. Geol.* **287**, 1–26.

Muller F., Seyler F. and Guyot J.- L. (1999) Utilisation d'imagerie radar (ROS) JERS-1 pour l'obtention de réseaux de drainage. Exemple du Rio Negro (Amazonie). *International Symposium on Hydrological and Geochemical Processes in Large Scale River Basins*, Manaus, Brazil.

Nelson D., Tréguer P., Brzezinski M., Leynaert A. and Quéguiner B. (1995) Production and dissolution of biogenic silica in the ocean: revised global estimates, comparison with regional data and relationship to biogenic sedimentation. *Global Biogeochem. Cycles* **9**, 359–372.

Opfergelt S., Cardinal D., Henriet C., Draye X., André L. and Delvaux B. (2006) silicon isotopic fractionation by banana (*Musa* spp.) grown in a continuous nutrient flow device. *Plant Soil* **285**, 333–345.

Opfergelt S., Delvaux B., André L. and Cardinal D. (2008) Plant silicon isotopic signature might reflect soil weathering degree. *Biogeochemistry* **91**, 163–175.

Opfergelt S., Georg R., Delvaux B., Cabidoche Y.-M., Burton K. and Halliday A. (2012) Silicon isotopes and the tracing of desilication in volcanic soil weathering sequences, Guadeloupe. *Chem. Geol.* **326–327**, 113–122.

Pardé M. (1947) *Fleuves et Rivières*. Armand Colin, Paris.

Ragueneau O., Savoye N., Del Amo Y., Cotten J., Tardiveau B. and Leynaert A. (2005) A new method for the measurement of biogenic silica in suspended matter of coastal waters: using Si:Al ratios to correct for the mineral interference. *Cont. Shelf Res.* **25**, 697–710.

Reynolds B. C., Aggarwal J., André L., Baxter D., Beucher C., Brzezinski M. A., Engström E., Georg R. B., Land M., Leng M. J., Opfergelt S., Rodushkin I., Sloane H. J., van den Boorn S. H. J. M., Vroon P. Z. and Cardinal D. (2007) An inter-laboratory comparison of Si isotope reference materials. *J. Anal. At. Spectrom.* **22**, 561–568.

Richey J., Mertes L., Dunne T., Victoria R., Forsberg B., Tancredi A. and Oliveira E. (1989) Sources and routing of the Amazon River flood wave. *Global Biogeochem. Cycles* **3**, 191–204.

Savage P. S., Georg R. B., Williams H. M., Turner S., Halliday A. N. and Chappell B. W. (2012) The silicon isotope composition of granites. *Geochim. Cosmochim. Acta* **92**, 184–202.

Savage P. S., Georg R. B., Williams H. M. and Halliday A. N. (2013) Silicon isotopes in granulite xenoliths: insights into isotopic fractionation during igneous processes and the composition of the deep continental crust. *Earth Planet. Sci Lett.* **365**, 221–231.

Sondag F., Guyot J. L., Moquet J. S., Laraque A., Adele G., Cochonneau G., Doudou J. C., Lagane C. and Vauchel P. (2010) Suspended sediment and dissolved load budgets of two Amazonian rivers from the Guiana shield: Maroni river at Langa Tabiki and Oyapock riverat Saut Maripa (French Guiana). *Hydrol. Process.* **24**, 1433–1445.

Stallard R. (1980) Major element geochemistry of the Amazon River system. Ph. D. thesis, Massachusetts Inst. Technol.

Stallard R. F. and Edmond J. M. (1981) Geochemistry of the Amazon 1. Precipitation chemistry and the marine contribution to the dissolved load at the time of peak discharge. *J. Geophys. Res.* **86**, 9844–9858.

Stallard R. F. and Edmond J. M. (1983) Geochemistry of the Amazon 2. The influence of geology and weathering environment on the dissolved load. *J. Geophys. Res.* **88**, 9671–9688.

Stallard R. F. and Edmond J. M. (1987) Geochemistry of the Amazon 3. Weathering chemistry and limits to dissolved inputs. *J. Geophys. Res.* **92**, 8293–8302.

Tardy Y., Bustillo V., Roquin C., Mortatti J. and Victoria R. (2005) The Amazon. Bio-geochemistry applied to river basin management: part I. Hydro-climatology, hydrograph separation, mass transfer balances, stable isotopes, and modelling. *Appl. Geochem.* **20**, 1746–1829.

Tardy Y. (1971) Characterization of the principal weathering types by the geochemistry of waters from some European and African crystalline massifs. *Chem. Geol.* **7**, 253–271.

Tollefson J. (2011) Environment: a struggle for power. *Nature* **479**, 160–161.

Tréguer P. J. and De La Rocha C. L. (2013) The world ocean silica cycle. *Annu. Rev. Mar. Sci.* **5**, 477–501.

Tréguer P. J. and Pondaven P. (2000) Silica control of carbon dioxide. *Nature* **406**, 358–359.

van den Boorn S., Vroon P. and Bergen M. (2009) Sulfur-induced offsets in MC-ICP-MS silicon-isotope measurements. *J. Anal. At. Spectrom.* **24**, 1111–1114.

Wille M., Sutton J., Ellwood M., Sambridge M., Maher W., Eggins S. and Kelly M. (2010) Silicon isotopic fractionation in marine sponges: a new model for understanding silicon isotopic variations in sponges. *Earth Planet. Sci. Lett.* **292**, 281–289.

Ziegler K., Chadwick O. A., Brzezinski M. A. and Kelly E. F. (2005a) Natural variations of δ^{30}Si ratios during progressive basalt weathering, Hawaiian Islands. *Geochim. Cosmochim. Acta* **69**, 4597–4610.

Ziegler K., Chadwick O. A., White A. F. and Brzezinski M. A. (2005b) δ^{30}Si systematics in a granitic saprolite, Puerto Rico. *Geology* **33**, 817–820.

Associate editor: Jerome Gaillardet